Fourier space approach to the classical density functional theory for multi-Yukawa and square-well fluids

Stepan P. Hlushak,[1,2,a)] Clare McCabe,[3] and Peter T. Cummings[1,4]
[1]*Department of Chemical and Biomolecular Engineering, Vanderbilt University, Nashville, Tennessee 37235, USA*
[2]*Institute for Condensed Matter Physics, Svientsitskoho 1, 79011 Lviv, Ukraine*
[3]*Department of Chemical and Biomolecular Engineering and Department of Chemistry, Vanderbilt University, Nashville, Tennessee 37235, USA*
[4]*Center for Nanophase Materials Sciences, Oak Ridge National Laboratory, Oak Ridge, Tennessee 37831, USA*

(Received 2 June 2012; accepted 17 August 2012; published online 11 September 2012)

We present a Fourier space density functional approach for hard particles with attractive interactions, which is based on a previously developed two-dimensional approach [S. Hlushak, W. Rżysko, and S. Sokołowski, J. Chem. Phys. **131**, 094904 (2009)] for hard-sphere chains. The interactions are incorporated by means of a three-dimensional Fourier image of the direct correlation function that is obtained from the first-order mean-spherical approximation. In order to improve the computational efficiency, we make extensive use of fast Fourier transforms for calculating density convolution integrals. A two-dimensional implementation of the new density functional approach, based on the expansion of the functional around the bulk fluid density, is used to study structure and adsorption of two model fluids in narrow cylindrical pores. We also investigate two methods that improve the accuracy of the theory as compared to the conventional DFT approach, which expands the free energy functional around the bulk fluid density: One a variant of the reference fluid density functional theory used by Gillespie *et al.* [Phys. Rev. E **68**, 031503 (2003)], and the second a weighted density approach with energy route thermodynamics. Results from these two methods are compared to the conventional approach and also to the results of Monte Carlo simulations. We find that the method of Gillespie *et al.* and the weighted density approach with energy route thermodynamics yield significant improvement over the conventional approach. © *2012 American Institute of Physics*. [http://dx.doi.org/10.1063/1.4749381]

I. INTRODUCTION

Porous materials have numerous applications in many branches of modern science and technology, such as membranes, separations, catalysis, and gas storage.[1–4] The successful application of porous materials requires a precise characterization of their structural properties, as well as an understanding of the physical and chemical behavior of the fluids adsorbed inside the pores. In turn, this requires a reliable theoretical method for the prediction of the structural and thermodynamic properties of confined fluids. While there are many methods employed for the study of confined fluids, the most commonly used theoretical methods are classical density functional theory (DFT) and molecular simulations.[5]

Classical DFT[6,7] is a generic method of statistical mechanics, applicable to both uniform and inhomogeneous systems, that retains the microscopic details of the macroscopic system at significantly lower computational cost as compared to molecular simulations. However, the accuracy and robustness of DFT is dependent on the analytical free-energy functionals and correlation functions used and often the lack of analytical expressions forces investigators to use mean field theories to account for attractive interactions,[8–10] reducing the accuracy of the approach. In the current work, we attempt to develop more accurate schemes by utilizing direct correlation functions (DCFs)[11,12] obtained from the first-order mean-spherical approximation (FMSA) for the square-well (SW)[13,14] and Lennard-Jones-like multi-Yukawa fluids (MY).[15] In particular, we extend a recently proposed density functional technique[16] for calculating the adsorption of hard chains into cylindrical pores and other complex pore geometries, to include attractive interactions between the chains and study the adsorption of SW and MY fluids into cylindrical pores.

In many DFT approaches[17–19] to adsorption, in which an adsorbed phase is in equilibrium with a bulk phase, the DCF is calculated at a reference density (in the simplest case, the bulk fluid density), and enters the free energy (functional) expression through the third term of the density expansion of the attraction part of the functional (see Sec. II A, Eq. (10)). The latter is truncated after the third term[20,21] and used as an approximation in the actual calculations. One disadvantage of this truncation is that the accuracy of the expansion decreases as the difference in the adsorbed phase and reference densities increases. To partially overcome this problem, we employ a variant of the reference fluid density functional approach proposed by Gillespie *et al.*[22] In our case, the reference density is uniform and assumed to be the fluid density averaged over the pore volume. This approximation should be applicable in cases of strong desorption/adsorption, when

a)Electronic mail: stepan.hlushak@gmail.com.

the density difference between the bulk and adsorbed fluids is significant.

Another important factor in the application of DFT to complex systems is a computational scheme that can be implemented numerically in multiple dimensions to determine the equilibrium density profile, which is formulated as a minimization of the grand potential functional and results in the need to solve the Euler-Lagrange equation.[23,24]

While several approaches[25–27] have been proposed for solving this equation, in this work, we employ a Picard-like iteration method[28] that does not require second derivatives of the free energy density functional and therefore is simpler to implement than other approaches. Furthermore, to speed up the calculation of the multidimensional density convolution integrals, they are integrated in Fourier space using convolution theorem and multi-dimensional Fourier transforms that can be computed efficiently via fast Fourier transforms as proposed by Frink *et al.*[26] This approach has proven to be more robust than the real-space based techniques and also simplifies the incorporation of attractive interactions into the scheme, since the DCF enters the expressions as a three-dimensional Fourier transform and therefore has a much simpler form than in real space.[11,12]

The aim of this work is therefore to combine several state-of-the-art techniques in DFT and solution methodology to develop a computationally efficient and accurate method for the quantitative modeling of fluid adsorption into nanoporous materials. The paper is organized as follows. In Sec. II, we present the model for the adsorbing fluids and the adsorbate, as well as the density functional theories being used. In order to evaluate the accuracy of the theories, we perform Monte Carlo simulations for comparison to the theoretical calculations, as described in Sec. III. The results obtained from the theory and simulations are compared in Sec. IV, and conclusions are summarized in Sec. V.

II. MODEL AND THEORY

A. Model

We consider a model fluid composed of spherical molecules that interact with each other through a hard-sphere plus an attractive potential. The attractive potential is represented by either a SW

$$u_{sw}(r) = \begin{cases} \infty, & r < \sigma \\ -\varepsilon, & \sigma < r < \lambda\sigma \\ 0, & r > \lambda\sigma, \end{cases} \tag{1}$$

or a MY

$$u_{mY}(r) = \begin{cases} \infty, & r < \sigma \\ \sum_i \varepsilon_i \sigma e^{-z_i(r-\sigma)}/r, & r > \sigma \end{cases} \tag{2}$$

potential.

The molecules are confined in cylindrical pores with hard and attractive walls. Thus, the external potential V_{ext} acting on each molecule in the case of pores with hard walls is assumed to be

$$V_{ext}(r) = \begin{cases} \infty, & r > R \\ 0, & \text{otherwise}, \end{cases} \tag{3}$$

where r is a distance from the center of the pore and R is the effective radius of a cylindrical pore.

In the case of attractive walls, the potential is given by

$$V_{ext}(r) = \begin{cases} \infty, & r > R, \\ -\varepsilon_{wall}, & R \geq r > R - \lambda_{wall}, \\ 0, & \text{otherwise}, \end{cases} \tag{4}$$

where ε_{wall} is the depth of the wall potential well and λ_{wall} is the width of the well.

We choose wall potentials that are quite simple (hard walls with and without SW attraction) as model systems for evaluating the accuracy of the proposed DFT approaches in comparison with Monte Carlo simulation results.

To test the theory we examined four different pore sizes, corresponding to pore radii (R) of 1.5σ and 2.5σ, as well as the effect of variations in the strength of the wall-fluid attraction with the following wall-fluid well depths considered: $\varepsilon_{wall} = 0$, $\varepsilon = \varepsilon$, $\varepsilon_{wall} = 2\varepsilon$, and $\varepsilon_{wall} = 3\varepsilon$, which correspond to repulsive, slightly attractive, moderately attractive, and highly attractive walls, respectively. The width of the wells in all cases was $\lambda_{wall} = \sigma$.

B. General relations and reference system

In the grand canonical ensemble, the thermodynamic properties of an inhomogeneous fluid are fully described by the grand potential functional

$$\Omega[\rho(\mathbf{r})] = F[\rho(\mathbf{r})] + \int d\mathbf{r}\rho(\mathbf{r})(V_{ext}(\mathbf{r}) - \mu), \tag{5}$$

where the square brackets denote functional dependence on the local number density $\rho(\mathbf{r})$ of molecules, μ is the chemical potential in the ensemble, and $F(\mathbf{r})$ is the free energy functional. The latter is expressed as a sum of contributions from an ideal-gas term and two excess terms that represent the repulsive and attractive interactions

$$F[\rho(\mathbf{r})] = F_{id}[\rho(\mathbf{r})] + F_{hs}[\rho(\mathbf{r})] + F_{att}[\rho(\mathbf{r})]. \tag{6}$$

The ideal-gas contribution can be expressed exactly as

$$\beta F_{id}[\rho(\mathbf{r})] = \int d\mathbf{r}\rho(\mathbf{r})[\ln(\rho(\mathbf{r})\Lambda^3) - 1], \tag{7}$$

where $\beta = 1/k_bT$; however, the excess terms can only be approximated.

The contribution due to the hard-sphere repulsive interactions, $F_{hs}[\rho(\mathbf{r})]$, is represented by the modified fundamental measure theory[29,30]

$$\beta F_{hs}[\rho(\mathbf{r})] = \int d\mathbf{r}\Phi_{hs}(\mathbf{r}) \tag{8}$$

where

$$\Phi_{hs} = -n_0 \ln(1 - n_3) + \frac{n_1 n_2 - \mathbf{n}_1 \cdot \mathbf{n}_2}{1 - n_3} + n_2^3(1 - 3\xi^2)\frac{n_3 + (1 - n_3)^2 \ln(1 - n_3)}{36\pi n_3^2(1 - n_3)^2}, \tag{9}$$

and the quantity ξ is defined as $\xi = |\mathbf{n}_2(\mathbf{r})|/n_2(\mathbf{r})$. In the above $n_i, i = 0, 1, 2, 3$ and $\mathbf{n}_i$, $i = 1, 2$ are the weighted

densities that are given as convolutions of the total density, with the corresponding weight functions of the fundamental measure theory. For their definitions and evaluation the reader is directed to Refs. 29 and 31and Appendix A of Ref. 26.

In Subsections II C and II D, we consider two definitions for the attractive interaction terms, which define mixed and energy-route approaches.

C. Mixed approach for attractive contribution

The free-energy term for attraction, $F_{att}[\rho(\mathbf{r})]$, is approximated by the expansion of the functional around some reference total density ρ_{ref} truncated to second-order:[20,21]

$$\beta F_{att}[\rho(\mathbf{r})] = \beta F_{att}(\rho_{ref}) + \beta\mu_{att}(\rho_{ref})\int d\mathbf{r}_1(\rho(\mathbf{r}_1)-\rho_{ref}) - \frac{1}{2}\int d\mathbf{r}_1 d\mathbf{r}_2 c_{att}(|\mathbf{r}_1-\mathbf{r}_2|;\rho_{ref}) \times(\rho(\mathbf{r}_1)-\rho_{ref})(\rho(\mathbf{r}_2)-\rho_{ref}), \quad (10)$$

where $F_{att}(\rho_{ref})$, $\mu_{att}(\rho_{ref})$, and $c_{att}(\mathbf{r}_1, \mathbf{r}_2; \rho_{ref})$ are the excess free energy, chemical potential, and direct correlation function (DCF), respectively, of the bulk fluid at a total density ρ_{ref}. In the current work these quantities are evaluated using the FMSA.[11,12,14] A detailed description of the FMSA is given in the Appendix. In the above functional the free energy $F_{att}(\rho_{ref})$ and the chemical potential $\mu_{att}(\rho_{ref})$ correspond to the energy route to the thermodynamics, while the DCF represents the compressibility route. It should be noted that the accuracy of the functional is dictated by the accuracy of the DCF. This can be seen by noting that the FMSA compressibility route results in a polynomial of the first order in β, while the FMSA energy route results in a second-order polynomial in β (see Eq. (A1)). Hence, expansion of the DCF in β is of lower order than the other terms in the functional and so is the term limiting the accuracy of the functional.

There are several options for choosing the reference total density (ρ_{ref}) that appears in Eq. (10). One of the simplest, and most commonly used, choices is to define the reference density as the density of the bulk fluid, ρ_b, with which the inhomogeneous fluid is in equilibrium. However, such an approach is likely to fail in cases when the density of the inhomogeneous fluid differs significantly from the bulk density. This is primarily because the expansion in Eq. (10) is inaccurate for cases of significant density differences which occur with fluids confined in highly attractive pores; but also this is due to inaccuracies in the DCF. In order to minimize density differences, we use the following as the reference density,

$$\rho_{ref} = \frac{1}{V_{pore}}\int_{V_{pore}} d\mathbf{r}'\bar{\rho}(\mathbf{r}'), \quad (11)$$

which is an average over the pore volume of a smoothed weighted density $\bar{\rho}(\mathbf{r})$ that is obtained by convolution of the total density with a normalized function, in this case $\omega_0(\mathbf{r})$,

$$\bar{\rho}(\mathbf{r}) = \int \rho(\mathbf{r}')\omega_0(|\mathbf{r}-\mathbf{r}'|). \quad (12)$$

To reduce the computational complexity we have chosen this function to have a similar form as that given by (20), but with the DCFs evaluated at $\rho = 0$,

$$\omega_0(\mathbf{r}) = \frac{c_{att}(r;\rho=0)}{\int c_{att}(r;\rho=0)d\mathbf{r}}. \quad (13)$$

Chosen in this way, the function is clearly normalized to unity and is ranged similarly to the interaction potential.

Since the total density profile depends on the reference fluid density, which in turn depends on the total density profile, the calculation must be iterated self-consistently, with ρ_{ref} computed at each iteration until convergence is achieved. Such a method may be viewed as a variant of the reference fluid density functional approach of Gillespie *et al.*;[22] in our case, the reference fluid density is also a functional of the total density, but is held constant over the pore volume. There is also a computational advantage to maintaining a uniform reference fluid density: since the numerical approach is based on the application of fast Fourier transforms and the DCF depends on the reference fluid density, this allows the calculation of the convolution of the DCF with the density difference only once for the entire pore volume.

The equilibrium properties are obtained by minimizing the grand potential functional (Eq. (5)), with respect to the number density profile $\rho(\mathbf{r})$. By taking a functional derivative of Eq. (5) and noting that it should be zero at the minimum, we obtain

$$\rho(\mathbf{r}) = \frac{1}{\Lambda^3}\exp\{-\beta V_{ext}(\mathbf{r}) + \beta\mu_{id}(\rho_b) + \left(\beta\mu_{hs}(\rho_b) - \beta\frac{\delta F_{hs}[\rho(\mathbf{r})]}{\delta\rho(\mathbf{r})}\right) + \left(\beta\mu_{att}(\rho_b) - \beta\frac{\delta F_{att}[\rho(\mathbf{r})]}{\delta\rho(\mathbf{r})}\right)\} \quad (14)$$

where

$$\beta\frac{\delta F_{att}[\rho(\mathbf{r})]}{\delta\rho(\mathbf{r})} = \beta\mu_{att}(\rho_{ref}) - \int d\mathbf{r}_1 c_{att}(|\mathbf{r}_1-\mathbf{r}|;\rho_{ref})(\rho(\mathbf{r}_1)-\rho_{ref}), \quad (15)$$

and the chemical potentials $\mu_{id}(\rho_b)$, $\mu_{hs}(\rho_b)$ and $\mu_{att}(\rho_b)$ are contributions to the chemical potential of the bulk fluid, viz.,

$$\mu(\rho_b) = \mu_{id}(\rho_b) + \mu_{hs}(\rho_b) + \mu_{att}(\rho_b), \quad (16)$$

with which the confined fluid is assumed to be in equilibrium.

At this point, three approximations can be introduced into the model. First, as described above, we can replace the reference fluid density ρ_{ref} in Eq. (15) with ρ_b and substitute it into Eq. (14), giving

$$\rho(\mathbf{r}) = \frac{1}{\Lambda^3}\exp\left\{-\beta V_{ext}(\mathbf{r}) + \beta\mu_{id}(\rho_b) + \left(\beta\mu_{hs}(\rho_b) - \beta\frac{\delta F_{hs}[\rho(\mathbf{r})]}{\delta\rho(\mathbf{r})}\right) + \int d\mathbf{r}_1 c_{att}(|\mathbf{r}_1-\mathbf{r}|;\rho_b)(\rho(\mathbf{r}_1)-\rho_b)\right\}, \quad (17)$$

which constitutes the bulk density expansion approach and does not require knowledge of the excess chemical potential

of the fluid; only the DCF is required. This approach will be denoted as the bulk density (BD) expansion approach.

In order to further simplify the treatment, we can also assume that the DCF in Eq. (17) is zero inside the hard core region. Since the FMSA DCF then satisfies the MSA closure condition, i.e., $c_{att}(r;\rho) = -\beta u(r)$ for $r > \sigma$, we recover the mean field (MF) approach, which does not require chemical potentials or DCF expressions. The two introduced approaches (BD and MF) are equivalent at $\rho_b \to 0$, since then $c_{att}(r;\rho_b) \to 0$ inside the hard core.

We also propose a more sophisticated approach based on the expansion of $F_{att}[\rho(\mathbf{r})]$ around the averaged pore density, according to relations (11), (14) and (15). We refer to this as the average density expansion (AD) approach. It should be noted, that since $F_{att}[\rho(\mathbf{r})]$ depends on ρ_{ref}, which is also the functional of $\rho(\mathbf{r})$, one can deduce that the functional derivative should be also taken from the $\rho_{ref}[\rho(\mathbf{r})]$ functional. But as was shown by Gillespie *et al.*,[22] the final expression for $\delta F_{att}[\rho(\mathbf{r})]/\delta\rho(\mathbf{r})$ does not depend on the functional dependence of $\rho_{ref}[\rho(\mathbf{r})]$, and is given by Eq. (15), wherein ρ_{ref} is constant.

The main purpose of the averaging procedure is to properly choose the reference fluid density at which the density difference in the convolution integral of Eq. (15) is small. This would reduce the error in the least accurate (last) term of Eq. (10) as much as possible, leading in turn to a more precise second order density expansion of the free energy functional. The simplest way to achieve this is to calculate an average of $\rho(\mathbf{r})$ over the integration volume. In our case, the average density is given by (11) and (12), where V_{pore} is the pore volume accessible to the particles, a space smaller than the physical pore volume.

D. Energy route approach for attractive contribution

In order to extend the theory to mimic accurate energy route thermodynamics, we employ a weighted density approximation proposed by Denton and Ashcroft[32] and later extended by Kim and Lee.[33] The attractive contribution to the free energy functional is approximated as

$$\beta F_{att}[\rho(\mathbf{r})] = \int d\mathbf{r}\rho(\mathbf{r})\beta f_{att}(\bar{\bar{\rho}}(\mathbf{r})), \tag{18}$$

where $\beta f_{att}(\rho) = \beta(u_1(\rho) + \beta u_2(\rho)/2)$ is the attractive free energy per particle, with $u_1(\rho)$ and $u_2(\rho)$ functions for the SW and MY fluids given by (A2), (A3) and (A11), (A12), respectively. The weighted density is calculated according to

$$\bar{\bar{\rho}}(\mathbf{r}) = \int \rho(\mathbf{r}')\omega_{att}(|\mathbf{r}-\mathbf{r}'|), \tag{19}$$

where

$$\omega_{att}(r) = \frac{c_{att}(r;\rho_{ref})}{\int c_{att}(r;\rho_{ref})d\mathbf{r}} \tag{20}$$

is a weight function normalized to unity and calculated from the attractive part of the DCF. In Fourier space the weight function is written in the following form:

$$\tilde{\omega}_{att}(k) = \frac{\tilde{c}_{att}(k;\rho_{ref})}{\tilde{c}_{att}(0;\rho_{ref})}, \tag{21}$$

where

$$\tilde{c}_{att}(0;\rho_{ref}) = \lim_{karrow0}\tilde{c}_{att}(k;\rho_{ref}) = 4\pi\int c_{att}(r;\rho_{ref})r^2dr \tag{22}$$

for the two model fluids studied herein.

The construction method of the functional given by Eq. (18) results in a combination of structural information from the FMSA DCF and accurate thermodynamics obtained from the FMSA energy route. The latter is reproduced by the functional in the case of a uniform density. Minimization of the grand potential functional yields Eq. (14), but now with the attractive contribution given by

$$\beta\frac{\delta F_{att}[\rho(\mathbf{r})]}{\delta\rho(\mathbf{r})} = \beta f_{att}(\bar{\rho}(\mathbf{r})) + \int \rho(\mathbf{r}')\beta\frac{\partial f_{att}(\bar{\rho}(\mathbf{r}'))}{\partial\bar{\rho}(\mathbf{r}')}\omega_{att}(|\mathbf{r}-\mathbf{r}'|)d\mathbf{r}'. \tag{23}$$

As seen in Sec. II D, the functional depends on the reference fluid density (through the DCF) found in (20). We note here that again several further weighted density approximations could be applied, namely MF-EN (mean-field, energy route), BD-EN (bulk density, energy route), and AD-ER (average density, energy route), which differ in the reference fluid density at which the direct correlation functions are evaluated. However, in forthcoming calculations we employ only the AD-ER theory as we expect that to be the most accurate of the three, since it uses the DCF evaluated at the average pore density.

When compared to other schemes[34–36] that account for the attractive interactions, the approaches presented here are more convenient, since the DCFs depend on the reference fluid density, which in our case is constant. Therefore, the convolution of the correlation function can be straightforwardly calculated in Fourier space using convolution theorem. This should not be possible in cases when the correlation function depends on the density, which is position dependent, as in the above mentioned schemes.[35,36]

E. The FMSA direct correlation function

All the thermodynamic and structural properties of the SW fluid are evaluated according to the FMSA theory. One of the challenges in the development of the current approach is the incorporation of the DCF structural information into an integration scheme based on the application of fast Fourier transforms. At first glance the task may seem prohibitive, since the DCF expression for the SW fluid has been shown to be rather lengthy;[11,12] however, because the DCF is required in the form of a three-dimensional Fourier transform the resulting expression for the DCF has a much simpler form than in r-space. This constitutes an additional advantage over real-space approaches, where the DCF formula implementation is more complex and computationally more expensive.

The three-dimensional Fourier transform of the DCF $c_{att}(|\mathbf{r}_1 - \mathbf{r}_2|; \rho_{ref})$ from expansion (10), is given by

$$\tilde{c}_{att}(k;\rho) = \frac{4\pi}{k}\int_0^\infty dr\, \sin(kr) r c_{att}(r;\rho) = \frac{2\pi}{ik}[\hat{c}_{att}(-ik\sigma;\rho) - \hat{c}_{att}(ik\sigma;\rho)], \quad (24)$$

where

$$\hat{c}_{att}(s;\rho) = \beta\varepsilon(1-\eta)^4\sigma^2\hat{Q}_0^2(-s)\hat{p}(s) \quad (25)$$

is the Laplace transform of the DCF; expressions for $\hat{Q}_0(s)$ and $\hat{p}(s)$ are given in the Appendix.

Since the DCF is radially symmetric and therefore the Fourier transform depends only on k, it can be tabulated into a one-dimensional array and then interpolated onto a multi-dimensional grid. Thus, in the multi-dimensional implementation of the AD approach, the recalculation of the DCF at every Picard iteration is not expensive relative to the evaluation of the convolution integrals.

The convolution integrals, on the other hand, are calculated using fast Fourier transform, which scales as $N \log N$ with the number of grid points N. In a real-space approach, the convolution of the direct correlation function with the density difference in (15) scales as N^2 in the case of the long-ranged DCF, or as NN_c when the DCF can be approximately set to zero above some cutoff distance. In the latter case N_c is the number of grid points in the volume of the cutoff sphere of the DCF, and should be proportional to the number of grid points N. Evidently, the Fourier space approach should offer performance increase for large N and N_c but for the general case the performance gain/loss will depend on the ratio between N_c and $\log N$. More detailed analysis of the asymptotic behavior of the Fourier-space and real-space approaches for the system of hard spheres was performed by Sears and Frink.[26]

III. SIMULATION DETAILS

To test the theoretical predictions, we have performed grand canonical Monte Carlo (GCMC) simulations of SW and MY fluids adsorbed into cylindrical pores. GCMC algorithms from Frenkel and Smith[37] were used with additional geometric constraints (infinite external potential) added to mimic a hard cylindrical pore.

The GCMC simulations, performed at fixed temperature and chemical potential, result in a chemical potential versus average density dependence. This dependence was obtained for all pores including the case of the bulk fluid. The latter is simply the bulk fluid chemical potential and is compared to the FMSA predictions for two model fluids in Fig. 2. The GCMC results are presented in the form of adsorption isotherms for different pore sizes in Figs. 4 and 7(a)–7(d) and in the form of radial density profiles in Figs. 3(a), 3(b), 5(a), 5(b), 6(a), and 6(b) to illustrate the in-pore structure. The density profiles were sampled at specific average pore packing fractions ($\eta = 0.1$, 0.2, and 0.3). In order to obtain the corresponding input chemical potentials, the adsorption isotherm, obtained from simulation, was interpolated and evaluated at the required average pore packing fractions. The obtained chemical potential was then used as an input into the subsequent simulation to determine the density profile.

The volume of the simulation box was always $10^3\sigma^3$ for both the bulk and inhomogeneous systems, which implies that the pore length is different for pores of different width, while the volume remains constant. Thus, for example, the box size for a pore of radius $R = 1.5\sigma$ was $3\sigma \times 3\sigma \times 111\sigma$. Standard periodic boundary conditions were applied along the cylindrical pore axis. The cutoff radius for the multi-Yukawa potential was set to 3σ.

A Monte Carlo step consisted of an attempt to insert the molecule, an attempt to remove the molecule, or an attempt to change the position of a randomly selected molecule, with probabilities of selecting a particular move: 25%, 25%, and 50%, respectively. The maximum particle displacement was adjusted during the simulation several times in order to reach the acceptance probability of 50%.

1×10^7 Monte Carlo steps were performed to allow each system to reach equilibrium before production runs of at least 1×10^8 additional Monte Carlo steps were carried out. The average density of the fluid inside the pore and the radial density profiles were calculated by determining the number of particles and their radial distribution histogram inside the pore every 2500 steps and then averaging the summed values at the end of simulation.

IV. RESULTS AND DISCUSSION

For the two systems studied, we consider a SW fluid with width $\lambda = 1.5$ and a MY fluid that mimics the Lennard-Jones potential. Both are confined in cylindrical pores with hard and SW walls. The MY fluid interacts according to a two-Yukawa potential of the following form:

$$u_{mYMY}(r) = \begin{cases} \infty, & r < \sigma \\ [\varepsilon_0 k_0 \sigma e^{-z_1(r-\sigma)} + \varepsilon_0 k_0 \sigma e^{-z_2(r-\sigma)}]/r, & r > \sigma, \end{cases} \quad (26)$$

where $z_1 = 2.9637/\sigma$, $z_2 = 14.0167/\sigma$, $k_0 = 2.1714$, and ε_0 is the energy parameter.

The confined fluids are assumed to be in equilibrium with a bulk fluid. Pore adsorption isotherms and density profiles were calculated using the proposed density functional approaches and GCMC simulation. The fluid density profiles, in our DFT implementation, were discretized and stored on a equally spaced grid with a step size of 0.025σ in both directions. Similarly, the DCF of the fluid was stored on a Fourier-space grid, with each point of the grid corresponding to a particular k-vector.

During the discretization of the circular cross section of the pore into rectangular grid, we are inevitably introducing numerical errors that will be proportional to the step size of the grid. However, we expect that the discretization errors are small when compared to the approximations made in the theories themselves. In order to perform numerically more accurate calculations in a cylindrical geometry, the reader is referred to the work of Malijevskỳ.[38]

Since all the key convolutions of our DFT approaches are performed in Fourier space, periodic boundary conditions are automatically applied. Therefore, a padding of width σ

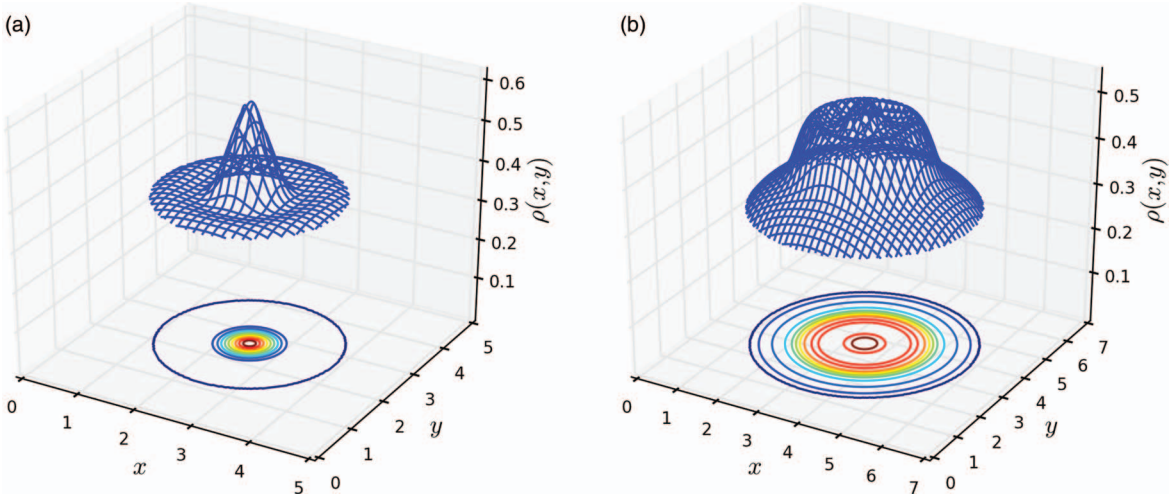

FIG. 1. Density profile for the SW fluid in a periodic box with a pore of radius $R^* = 1.5$ (a) and $R^* = 2.5$ (b) at an average pore density of $\rho^* = 0.4$ and a temperature of $T^* = 1.5$ as obtained from the BD theory.

was added to the edges of the DFT box to avoid interactions between particles in neighboring pores. Thus, the (two-dimensional) box, in the case of a pore of radius $R = 1.5\sigma$, has dimensions $5\sigma \times 5\sigma$ (see Fig. 1(a)), and the density of the fluid along the axis of the pore is assumed to be uniform. The distance between the neighboring pores in this case is 2σ, which is clearly enough for the SW particles not to interact with particles in other pores and is sufficient to neglect such effects for MY particles. Similar padding is used in the DFT calculations for other pores, which can be seen from the density profile of the SW fluid inside a pore of radius $R = 2.5\sigma$ shown in Fig. 1(b). Here the box size is $7\sigma \times 7\sigma$. As would be expected and can be seen from Figs. 1(a) and 1(b), the density profiles depend only on the radial distance from the center of the pore; therefore, it is more convenient to present the density profiles in the form of a radial dependence.

For additional details on the DFT calculations the reader is directed to previous work,[16] in which the analytical expressions for the Fourier transforms of the weight functions and other technical details are presented.

Before proceeding to the adsorption calculations, we first need to validate the bulk chemical potentials predicted by the FMSA theory, which are used as an input into the DFT calculations performed in grand canonical ensemble. In Fig. 2, the chemical potentials for the SW and MY fluids are presented at $T^* = 1.5$, where $T^* = T/\varepsilon$ is the dimensionless temperature and $\rho^* = \rho\sigma^3$ the dimensionless density. The selected temperature ($T^* = 1.5$) is supercritical for the studied model fluids, and, therefore, the vapor-liquid phase transition is not observed. As can be seen from the figure, excellent agreement is obtained between the FMSA theory and the GCMC simulations. Thus, one can conclude that the application of the FMSA thermodynamics for evaluation of the bulk chemical potentials, which are used as an input to the DFT iterations, is well justified.

The main results of this work are presented as follows. In Fig. 3 (MY fluids) and Figs. 5 and 6 (SW fluids), we provide density profiles of the fluids in cylindrical pores of different diameter; in Figs. 4 and 7(a)–7(d), we present adsorption isotherms for these systems. All profiles reported, both from the DFT calculations and the GCMC simulations, were calculated at $T^* = 1.5$ and compared at equal average pore densities. As a result, the chemical potentials (corresponding to the profiles of different DFT theories and simulation at the same average pore densities) are slightly different. The average pore densities, defined as

$$\rho_{av.} = \frac{1}{V_{pore}} \int_{V_{pore}} d\mathbf{r}\rho(\mathbf{r}), \tag{27}$$

are compared in the adsorption isotherm Figs. 4 and 7(a)–7(d). Calculations were performed for model fluids confined in cylindrical pores with radii $R = 1.5\sigma$ and 2.5σ and different fluid-wall attraction parameters. Representative adsorption isotherms are presented for the cases of $R = 1.5\sigma$ and

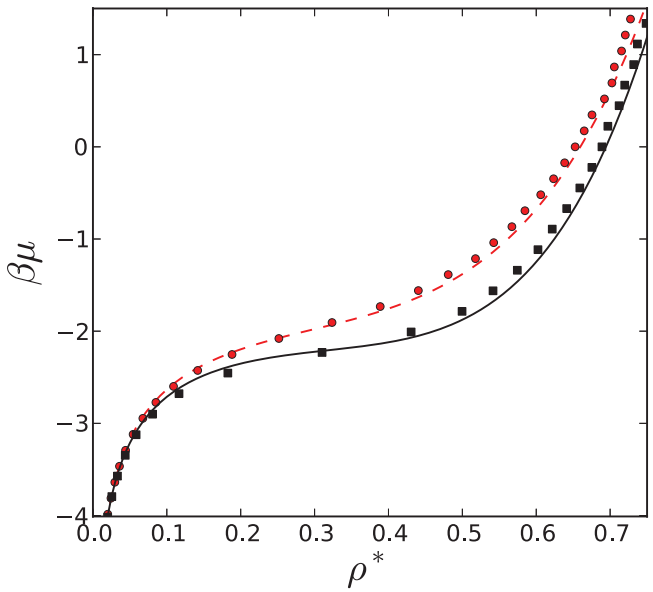

FIG. 2. Chemical potentials for the SW (black solid line and rectangles) and MY (red dashed line and circles) bulk fluids at $T^* = 1.5$ as obtained from the FMSA theory (lines) and GCMC simulations (symbols).

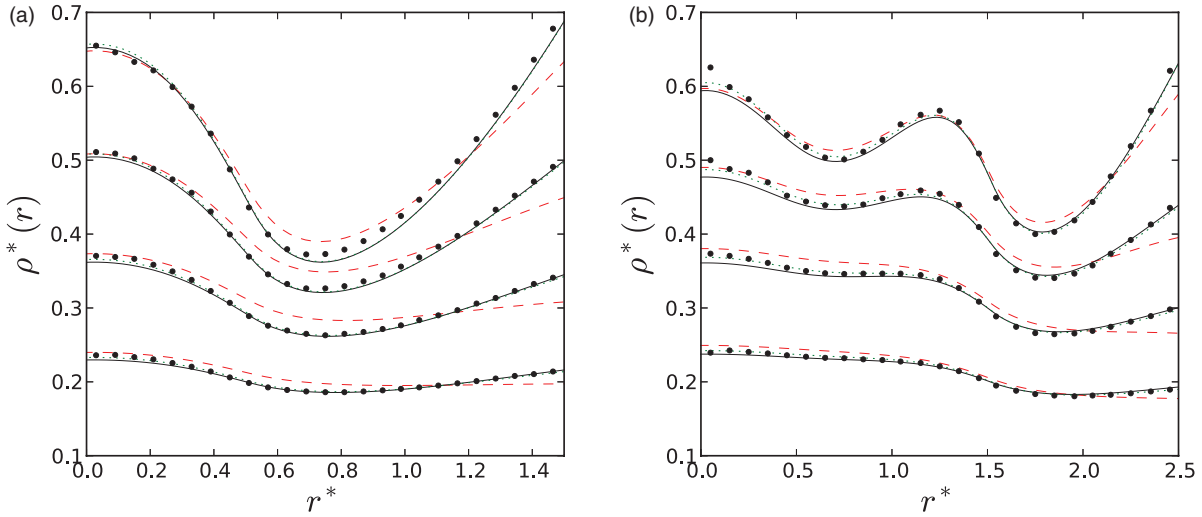

FIG. 3. Density profiles of the MY fluid in a hard cylindrical pore of radius $R^* = 1.5$ (a) and $R^* = 2.5$ (b) at $T^* = 1.5$ for several average pore densities as obtained from the AD (black solid lines), BD (red dashed lines), AD-ER (green dotted lines) theories, and GCMC simulations (symbols). The average pore densities that correspond to the profiles are $\rho^* = 0.4$, 0.3, and 0.2 (from top to bottom). r^* denotes the distance from the center of the pore.

2.5σ at different wall-fluid attraction strengths in Figs. 7(a)–7(d) for the SW fluid and in Fig. 4 for the MY fluid.

From the pore profiles for the MY fluid (Fig. 3), we observe that the BD theory provides good predictions of the density profiles and is in reasonable agreement with the MC simulation data for the excess adsorbed density isotherm, as shown in Fig. 4. However, the profiles predicted by AD and AD-ER theories are generally closer to the simulation results, which is clearly visible at contact near the wall. Moreover, adsorption isotherms, presented in Fig. 4, are more accurate at low densities, where the fluid is repelled from the pore. Taking into account that the density profiles from the BD theory are not very accurate, it is surprising that the isotherms are in good agreement at high densities.

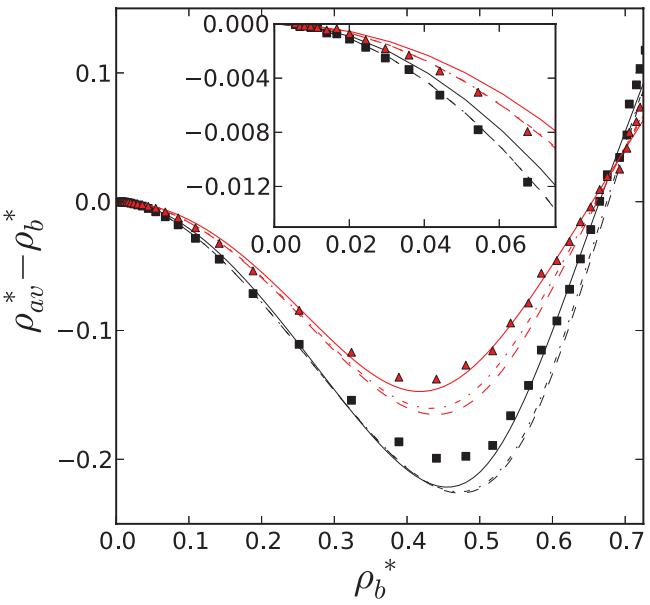

FIG. 4. Comparison of adsorption isotherms (average pore density vs. bulk density) for four different pores ($R^* = 1.5$, 2.0, 2.5, and 3.0) obtained from the BD theory (lines) and GCMC simulations (symbols) for the MY fluid at $T^* = 1.5$.

We now turn to the results for the SW fluid, which because of the longer-ranged nature of the SW potential provides density profiles and adsorption isotherms that are richer than those seen for the MY fluids; the differences between the theories can therefore be more fully revealed. As seen in Fig. 5, although each of the theories show a depletion of the fluid from the repulsive hard walls, there is a substantial difference in the density profiles. Most notable, the BD theory appears to be inaccurate in that it consistently overestimates the amount of absorbed fluid in the central region of the pore and underestimates the contact density at the wall. On the other hand, the AD theory shows significant improvement over the BD at low and intermediate densities; like the more accurate AD-ER theory, the AD appears to be in good agreement with the simulation profiles. At higher bulk densities all the theories are seen to underpredict the contact density at the wall. The AD-ER theory appears to provide the most accurate density profiles for all pore sizes and densities studied.

In Fig. 6 density profiles for pores with SW walls and $\varepsilon_{wall} = 3.0\varepsilon$ are presented. Each profile consists of enriched and depleted parts, located inside and outside the potential well, respectively, and are divided by quite a large discontinuity. One might expect that it will be difficult for the AD and AD-ER theories to describe such profiles, since their adaptive reference density is constrained to be uniform. Nevertheless, the uniform reference density is still closer to the actual pore density than the bulk density, and this enables the two advanced theories to better agree with the simulation profiles. For the wide pore (2.5σ) the different theoretical profiles almost coincide.

The excess average pore densities predicted by the theories are presented in Figs. 7(a)–7(d) for hard and increasingly attractive pore walls. The low density adsorption isotherms (see the inner plots of each figure) reveal the higher accuracy of the theories with the adaptive (averaged) reference density, which yields the most accurate agreement with the

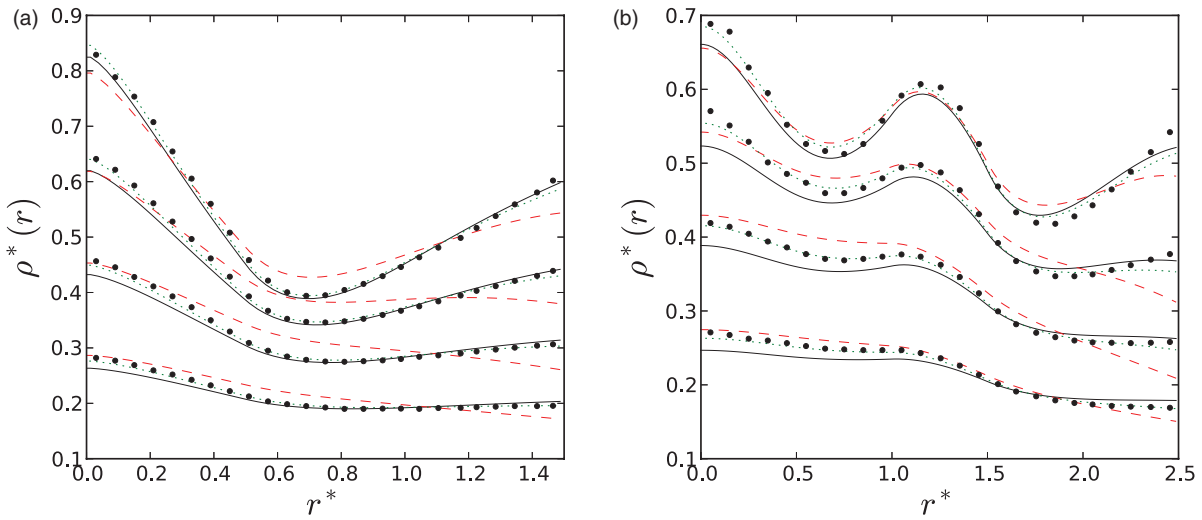

FIG. 5. Density profiles of the SW fluid in a hard cylindrical pore with $R^* = 1.5$ (a) and $R^* = 2.5$ (b), at $T^* = 1.5$ for several average pore densities as obtained from the AD (black solid lines), BD (red dashed lines), and AD-ER (green dotted lines) theories and GCMC simulations (symbols). The average pore densities that correspond to the profiles are $\rho^* = 0.5$, 0.4, 0.3, and 0.2 (from top to bottom). r^* denotes the distance from the center of the pore.

simulation results. The least accurate theory at low densities is the BD approach; for hard pores it overestimates the amount of the adsorbed fluid at low and intermediate densities and becomes more accurate only at higher densities, where the average pore density approaches the bulk value, while in the case of highly attractive pores the amount of adsorbed fluid is underestimated.

At intermediate and high densities the AD and AD-ER isotherms for the hard pores are quite close to each other but not really more accurate than the isotherm obtained from the BD theory (see Fig. 7(a)). The greatest advantage the AD and AD-ER theories offer are at low bulk density, where the fluid is repelled from the pore, and because of the adaptive reference density, this depletion is more correctly taken into account. Overall, the AD-ER theory seems to be more accurate for the narrowest pore (with $R = 1.5\sigma$), but its accuracy approaches that of the AD approach as the density decreases. The BD isotherm, on the other hand, provides the least accurate predictions for the narrowest pore ($R = 1.5\sigma$) at all densities, but, seems to give reasonable results for wider pores ($R = 2.5\sigma$) at higher density. Because the reference fluid density is uniform (constant), there is not much freedom to adapt to the actual density profile, so, it is not surprising that AD and AD-ER theories loose their accuracy as the pore volume increases. This is a consequence of the fact, that in our implementation of the DFT the reference density is kept uniform, so, as the pore becomes wider (infinite for single wall case), the accuracy of the AD approach tends to the BD case. A solution to this problem could be to use a nonuniform reference fluid density. But, as has been shown recently,[39] this is much

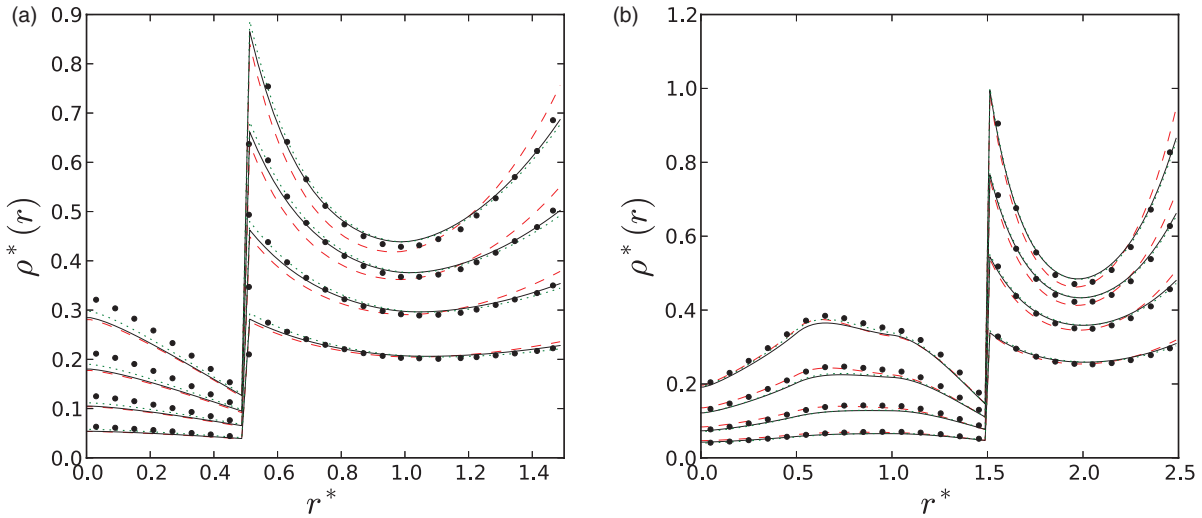

FIG. 6. Density profiles for the SW fluid adsorbed in a cylindrical pore with SW walls ($\varepsilon_{wall} = 3.0$, $\lambda_{wall} = \sigma$) and $R^* = 1.5$ (a) and $R^* = 2.5$ (b) at $T^* = 1.5$ for several average pore densities obtained from the AD (black solid lines), BD (red dashed lines), and AD-ER (green dotted lines) theories and GCMC simulations (symbols). The average pore densities that correspond to the profiles are $\rho^* = 0.5$, 0.4, 0.3, and 0.2 (from top to bottom). r^* denotes the distance from the center of the pore.

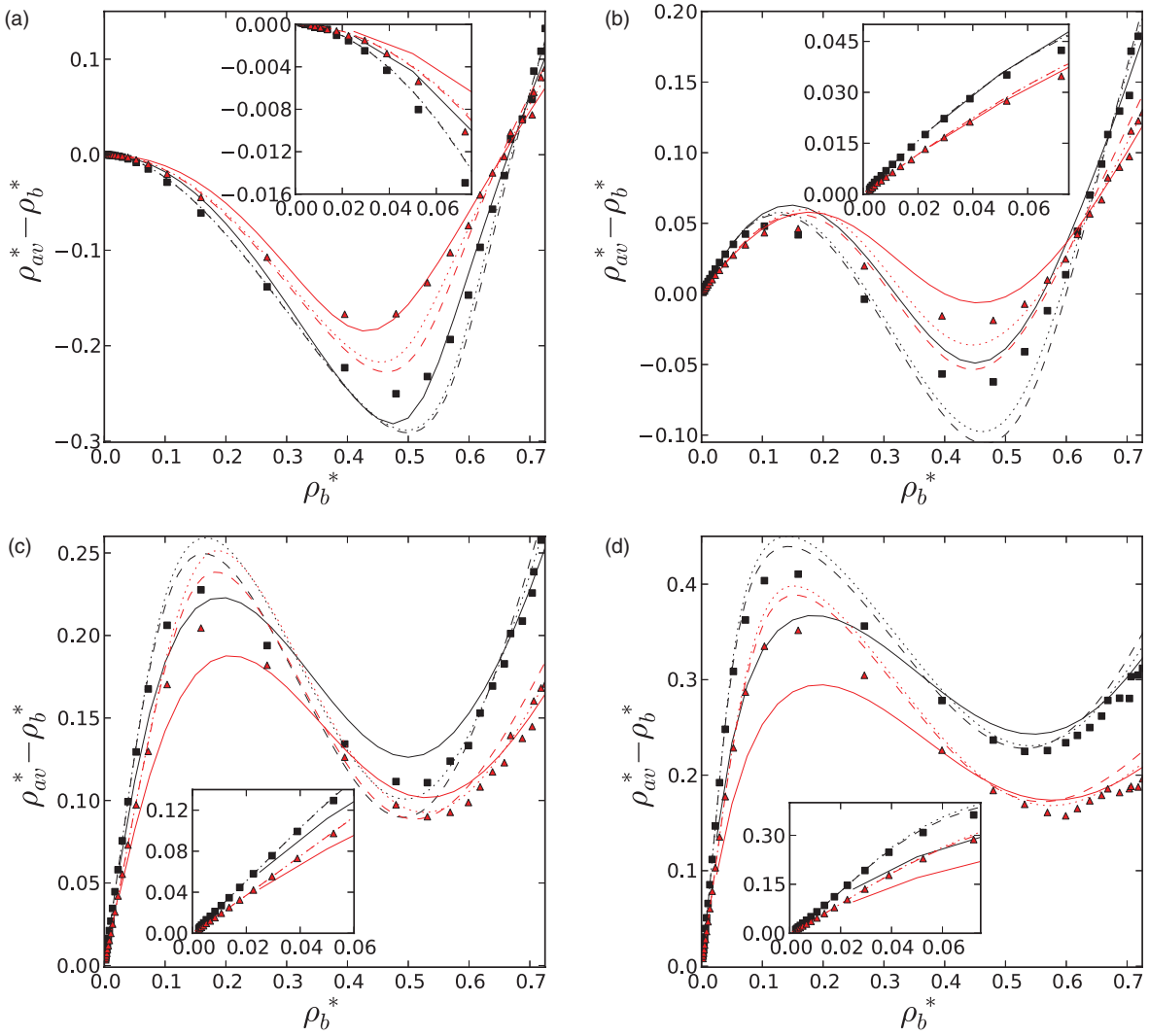

FIG. 7. Comparison of adsorption isotherms (excess average pore density vs. bulk density) for the SW fluid at $T^* = 1.5$ in two different ($R^* = 1.5$ (black color) and 2.5 (red color)) cylindrical pores as obtained from the AD (solid lines), BD (dashed lines), and AD-ER (dotted lines) theories and GCMC simulations (symbols). Walls are hard (a) and attractive with $\varepsilon_{wall} = 1.0\ \varepsilon$ (b), $\varepsilon_{wall} = 2.0\ \varepsilon$ (c), and $\varepsilon_{wall} = 3.0\ \varepsilon$ (d). The inset shows the low-density region of the plot.

more computationally expensive as the approach becomes incompatible with the Fourier-space integration approach, since it has to reevaluate the DCF and its convolution at every grid point, resulting in an algorithm whose complexity is proportional to the square of the number of grid points.

For lightly attractive pore with $\varepsilon_{wall} = \varepsilon$ (see Fig. 7(b)), the repulsive effect of the hard walls is roughly compensated for by the attractive potential well. The excess adsorbed density isotherm oscillates around zero, and consequently, the BD theory shows good agreement for this case. This is because the average pore density is always close to the bulk density, which is the reference density for the BD theory. The other two approaches give comparable results, slightly underestimating the adsorption at intermediate densities

Adsorption isotherms for attractive pores with $\varepsilon_{wall} = 2\ \varepsilon$ and $\varepsilon_{wall} = 3\ \varepsilon$, as shown in Figs. 7(c) and 7(d), illustrate that the adaptive reference fluid density approaches are in better agreement with the simulation results as compared to the bulk density expansion approach (the BD theory). First, the higher adsorption rates at low densities (see insets) are more accurately predicted by the AD and AD-ER theories (i.e., the theories with the reference fluid density calculated as an average of pore volume). Second, the excess adsorption minimum at intermediate-high densities seems to also be more accurately captured. However, the accuracy of the two approaches seems to diminish slightly as the pore becomes wider, which is again a manifestation of the uniformity constraint of the reference fluid density, (i.e., since the reference density is kept uniform as the pore becomes wider the accuracy of the AD approach will tend to the BD case).

Mean relative errors for the average pore densities are compared with the Monte Carlo simulation data in Table I. The errors were calculated for the full adsorbed densities, instead of the excess adsorbed densities, since in the latter case the simulation data points, which are close to zero, will artificially have higher weight in the resulting error. Analysis of the errors reveals that the AD and AD-ER approaches are more accurate for the adsorption of the SW fluid, but are only slightly less accurate for the MY fluid (for which only a hard pore was studied).

TABLE I. Mean relative error[a] of the theoretical average adsorbed density of the MY and SW fluids when compared to the corresponding Monte Carlo simulation results. Errors are reported for the BD, AD, AD-ER theories, and pores of Figs. 4 and 7.

	MY fluid		SW fluid							
	$\varepsilon_{wall}=0$		$\varepsilon_{wall}=0$		$\varepsilon_{wall}=\varepsilon$		$\varepsilon_{wall}=2\varepsilon$		$\varepsilon_{wall}=3\varepsilon$	
Theory	$R=1.5$	$R=2.5$	$R=1.5$	$R=2.5$	$R=1.5$	$R=2.5$	$R=1.5$	$R=2.5$	$R=1.5$	$R=2.5$
BD	0.082	0.074	0.118	0.093	0.090	0.076	0.069	0.071	0.062	0.070
AD	0.090	0.082	0.065	0.049	0.036	0.027	0.023	0.023	0.023	0.025
AD-ER	0.087	0.078	0.057	0.039	0.031	0.021	0.023	0.025	0.029	0.027

[a]Mean relative error is given by $\delta\rho_{av}=\sum_i\left|\frac{\rho_{av,i}-\rho_{exp,i}}{\rho_{exp,i}}\right|$.

V. CONCLUSIONS

We have presented a variation of the Fourier-transform-based density functional approach that takes into account pair-wise attractive interactions between particles. All the density convolution integrals of the approach are evaluated in Fourier space by means of the fast Fourier transforms, which is expected to speed up the calculations.

Three different approximations for the free-energy terms responsible for taking into account the attractive interactions were formulated and validated by comparison against the results of grand canonical Monte Carlo simulations. The simplest approach, the bulk density (BD), uses the bulk fluid density as the reference density. In a more advanced approximation, the average density expansion approach (AD), a variant of the reference fluid density functional theory proposed by Gillespie *et al.*[22] with uniform reference fluid density is used. A third approach, the weighted density approximation of Denton and Ashcroft[32] (AD-ER), incorporates the more accurate FMSA energy route thermodynamics.

The performance of the approaches was tested for several nanopores and the most accurate found to be the AD-ER theory, followed by the AD approach, which for the cases studied is only slightly less accurate than the AD-ER approach; however, while these two theories offer advantages in accuracy over the BD theory, this is offset by their higher computational cost. The BD theory requires evaluation of the DCF only at the start of the iterations, while the AD approach re-evaluates the DCF at every Picard iteration. Furthermore, the AD-ER theory calculates additional thermodynamic functions (free energy and chemical potential) for every grid point at every Picard iteration. This calculation proves to be very costly for the SW fluid in the FMSA approximation and requires the use of an interpolation scheme for the thermodynamics, in which the density dependence of the chemical potential and free energy (at a particular temperature) is tabulated and then interpolated to get the corresponding values for every point of the grid.

An additional issue with the AD type approaches is the requirement of uniformity in the reference fluid density. Because of this, the density difference in the last term of Eq. (10) is more significant for wider pores, and as a result, we observe that the accuracy of the approach may degrade as wider pores are considered. In the limiting case of the infinitely wide pore the reference fluid density will approach the bulk fluid density and the AD approach will eventually become equivalent to the BD approach.

ACKNOWLEDGMENTS

S.H. and P.T.C. were supported by the U.S. Department of Energy (DOE), Office of Basic Energy Sciences, Geoscience Research Program, through Grant No. ERKCC72 to Oak Ridge National Laboratory, which is managed for DOE by UT Battelle, LLC under Contract No. DE-AC05-00OR22725. C.M.C. acknowledges support from the National Science Foundation (NSF) under Grant No. CBET-1067642.

APPENDIX A: FMSA THERMODYNAMICS

1. SW fluid

The Helmholtz free energy density obtained from the FMSA reads[32]

$$\frac{\beta F_{att}(\rho)}{V}=\beta\rho\left[u_1(\rho)+\frac{\beta u_2(\rho)}{2}\right], \tag{A1}$$

where V is the volume of the system, and

$$u_1(\rho)=-\varepsilon-12\varepsilon\eta\sum_{i=0}^{2}\frac{L(t_i)(\lambda t_i-1)e^{(\lambda-1)t_i}}{t_i S_1(t_i)} \tag{A2}$$

$$u_2(\rho)=-12\varepsilon^2\eta(1-\eta)^8\left\{\sum_{i=0}^{2}\left[\frac{M(-t_i)F_1(t_i)}{S^2(-t_i)}-\frac{M_1(-t_i)S(-t_i)-2M(-t_i)S_1(-t_i)}{S^3(-t_i)}F(t_i)\right]\right.$$
$$\left.+\sum_{i=0}^{2}\sum_{j=0}^{2}\left[F_1(t_i)F_1(t_j)-\frac{F(t_i)F_1(t_j)+F_1(t_i)F(t_j)}{t_i+t_j}+2\frac{F(t_i)F(t_j)}{(t_i+t_j)^2}\right]\frac{e^{(t_i+t_j)(\lambda-1)}}{t_i+t_j}\right\}. \tag{A3}$$

In the above equations $\eta = \pi\rho\sigma^3/6$ and t_j are roots of $S(t) = 0$ equation, and are given by

$$t_j = \frac{(-2\eta + (2\eta f)^{1/3}(y_+ c^j + y_- c^{-j}))}{1-\eta}, \quad j = 0, 1, 2, \tag{A4}$$

where

$$f = 3 + 3\eta - \eta^2, \tag{A5}$$

$$y_\pm = \left(1 \pm \left(1 + \frac{2\eta^4}{f^2}\right)^{1/2}\right)^{1/3}, \tag{A6}$$

$$c = e^{2\pi i/3}, \quad with \quad i^2 = -1. \tag{A7}$$

Yet undefined functions $L(t), S(t), F(t), M(t), S_1(t), F_1(t), M_1(t)$ and $S_2(t)$ are following:

$$L(t) = \left(1 + \frac{\eta}{2}\right)t + 1 + 2\eta, \tag{A8}$$

$$S(t) = (1-\eta)^2 t^3 + 6\eta(1-\eta)t^2 + 18\eta^2 t - 12\eta(1+2\eta), \tag{A9}$$

$$S_1(t) = 3(1-\eta)^2 t^2 + 12\eta(1-\eta)t + 18\eta^2,$$

$$S_2(t) = 6(1-\eta)^2 t + 12\eta(1-\eta),$$

$$M(t) = C(t) = \lambda t^5 - t^4, \quad C_1(t) = C'(t),$$

$$M_1(t) = C_1(t) + (\lambda - 1)C(t),$$

$$F(t) = \frac{M(t)}{S_1^2(t)}, \qquad F_1 = \frac{M_1(t)}{S_1^2(t)} - \frac{M(t)S_2(t)}{S_1^3(t)}.$$

The chemical potential is obtained by differentiating (A1) with respect to ρ. The resulting expressions are rather long but quite straightforward, so they are not presented here. We should also note that the chemical potential derivation requires evaluation of $\partial t_j/\partial\rho$ derivatives, so the care must be taken to include these. The formulas for SW fluid presented here are valid for $\lambda < 2$.

2. MY fluid

For the multi-Yukawa fluid, the expression for free energy density is similar to (A1),

$$\frac{\beta F_{att}(\rho)}{V} = \beta\rho\left[u_1(\rho) + \frac{\beta u_2(\rho)}{2}\right], \tag{A10}$$

with $u_1(\rho)$ and $u_2(\rho)$ given by

$$u_1(\rho) = -12\eta\sum_i \frac{\varepsilon_i L(z_i\sigma)}{(1-\eta)^2\hat{Q}_0(z_i\sigma)(z_i\sigma)^2}, \tag{A11}$$

$$u_2(\rho) = -12\eta\sum_i\sum_j \frac{\varepsilon_i\varepsilon_j}{(z_i\sigma + z_j\sigma)\hat{Q}_0^2(z_i\sigma)\hat{Q}_0^2(z_j\sigma)}, \tag{A12}$$

where

$$\hat{Q}_0(t) = \frac{S(t) + 12\eta L(t)e^{-t}}{(1-\eta)^2 t^3}, \tag{A13}$$

with $S(t)$ and $L(t)$ given by (A8) and (A9), respectively.

APPENDIX B: FMSA STRUCTURAL PROPERTIES

1. SW fluid

The DCF $c_{att}(|\mathbf{r}_1 - \mathbf{r}_2|; \rho_{ref})$, that enters expansion (10), is approximated by means of the FMSA theory.[11,12] Since the algorithm is based on the application of the Fourier transform, only the three-dimensional Fourier transform is required

$$\tilde{c}_{att}(k;\rho) = \frac{4\pi}{k}\int_0^\infty dr\,\sin(kr)rc_{att}(r;\rho) = \frac{2\pi}{ik}[\hat{c}_{att}(-ik\sigma;\rho) - \hat{c}_{att}(ik\sigma;\rho)], \tag{B1}$$

where

$$\hat{c}_{att}(s;\rho) = \beta(1-\eta)^4\sigma^2\hat{Q}_0^2(-s)\hat{p}(s) \tag{B2}$$

with $Q_0(s)$ given by (A13), and

$$\hat{p}(s) = -\varepsilon\sum_{i=0}^{2}\left\{\frac{F_2(t_i)}{(s+t_i)} - \frac{F(t_i)}{(s+t_i)^2}\right\}e^{-\lambda s} + \varepsilon\sum_{i=0}^{2}\left\{\frac{F_2(t_i)+F(t_i)(\lambda-1)}{(s+t_i)} - \frac{F(t_i)}{(s+t_i)^2}\right\}e^{(\lambda-1)t_i}e^{-s}, \tag{B3}$$

with

$$F_2(t) = \frac{C_1(t)}{S_1^2(t)} - \frac{C(t)S_2(t)}{S_1^3(t)}. \tag{B4}$$

Additionally to (B1) one should also require $\tilde{c}_{att}(0)$, which reads

$$\begin{aligned}\tilde{c}_{att}(0) = \lim_{k\to 0}\tilde{c}_{att}(k) = 4\pi\beta\varepsilon\sigma^3(1+2\eta)^2\Bigg[&-\sum_{i=0}^{2}\left\{\frac{F_1(t_i)(\lambda t_i+1)}{t_i^2} - \frac{F(t_i)(\lambda t_i+2)}{t_i^3}\right\}\\ &+\sum_{i=0}^{2}\left\{\left[F_1(t_i) + F(t_i)(\lambda-1)\right]\frac{t_i+1}{t_i^2} - \frac{F(t_i)(t_i+2)}{t_i^3}\right\}e^{(\lambda-1)t_i}\Bigg]\\ -12\pi\beta\varepsilon\sigma^3\eta(1+2\eta)\Bigg[&-\sum_{i=0}^{2}\left\{\frac{F_1(t_1)}{t_i} - \frac{F(t_i)}{t_i^2}\right\}\\ &+\sum_{i=0}^{2}\left\{\frac{F_1(t_i)+F(t_i)(\lambda-1)}{t_i} - \frac{F(t_i)}{t_i^2}\right\}e^{(\lambda-1)t_i}\Bigg].\end{aligned} \tag{B5}$$

2. MY fluid

For the multi-Yukawa fluid the general formulas (B1) and (B2) remain unchanged, while $\hat{p}(s)$ changes to

$$\hat{p}(s) = \sum_i \frac{\varepsilon_i e^{-s}}{\hat{Q}_0^2(s)(s + z_i\sigma)}. \tag{B6}$$

Now, the $\tilde{c}_{att}(0)$ is

$$\tilde{c}_{att}(0) = \lim_{k\to 0} \tilde{c}_{att}(k) = \frac{4\pi\beta\sigma^3}{(1-\eta)^4} \sum_i \frac{\varepsilon_i}{\hat{Q}_0^2(z_i\sigma)} \times \left[(1+2\eta)^2 \frac{1+z_i\sigma}{(z_i\sigma)^2} - 3\eta(1+2\eta)\frac{1}{z_i\sigma}\right]. \tag{B7}$$

[1] K. Ishizaki, S. Komarneni, and M. Nanko, *Porous Materials: Process Technology and Applications* (Chapman and Hall, 1998), Vol. 4.
[2] M. Mulder, *Basic Principles of Membrane Technology* (Springer, 1996).
[3] A. Basile and F. Gallucci, *Membranes for Membrane Reactors: Preparation, Optimization and Selection* (Wiley, 2011).
[4] J. C. Janson, *Protein Purification: Principles, High Resolution Methods, and Applications* (Wiley, 2011).
[5] K. E. Gubbins, Y. C. Liu, J. D. Moore, and J. C. Palmer, Phys. Chem. Chem. Phys. **13**, 58 (2011).
[6] J. Wu and Z. Li, Annu. Rev. Phys. Chem. **58**, 85 (2007).
[7] J. Wu, AIChE J. **52**, 1169 (2006).
[8] O. Pizio, M. Borówko, W. Rżysko, T. Staszewski, and S. Sokołowski, J. Chem. Phys. **128**, 044702 (2008).
[9] X. Xu and D. Cao, J. Chem. Phys. **130**, 164901 (2009).
[10] A. V. Neimark, Y. Lin, P. I. Ravikovitch, and M. Thommes, Carbon **47**, 1617 (2009).
[11] Y. Tang, J Chem. Phys. **127**, 164504 (2007).
[12] S. Hlushak, A. Trokhymchuk, and S. Sokołowski, J Chem. Phys. **130**, 234511 (2009).
[13] Y. Tang and B. C.-Y. Lu, J. Chem. Phys. **99**, 9828 (1993).
[14] Y. Tang and B. C.-Y. Lu, J. Chem. Phys. **100**, 6665 (1994).
[15] Y. Tang and J. Wu, J. Chem. Phys. **119**, 7388 (2003).
[16] S. Hlushak, W. Rżysko, and S. Sokołowski, J. Chem. Phys. **131**, 094904 (2009).
[17] Z. Jin, Y. Tang, and J. Wu, J. Chem. Phys. **134**, 174702 (2011).
[18] J. Mi, Y. Tang, C. Zhong, and Y. G. Li, J. Chem. Phys. **124**, 144709 (2006).
[19] P. Bryk, W. Rżysko, A. Malijevský, and S. Sokołowski, J. Colloid Interface Sci. **313**, 41 (2007).
[20] T. V. Ramakrishnan and M. Yussouff, Phys. Rev. B **19**, 2775 (1979).
[21] A. D. J. Haymet and D. J. Oxtoby, J. Chem. Phys. **74**, 2559 (1981).
[22] D. Gillespie, W. Nonner, and R. S. Eisenberg, Phys. Rev. E **68**, 031503 (2003).
[23] J. P. Hansen and I. R. McDonald, *Theory of Simple Liquids* (Academic, 2006).
[24] In calculus of variations, the Euler-Lagrange equation, Euler's equation, or Lagrange's equation, is a differential equation whose solutions are the functions for which a given functional is stationary. See http://en.wikipedia.org/wiki/Euler-Lagrange_equation.
[25] L. J. D. Frink and A. G. Salinger, J. Comput. Phys. **159**, 407–424 (2000).
[26] M. P. Sears and L. J. D. Frink, J. Comput. Phys. **190**, 184 (2003).
[27] A. G. Salinger and L. J. D. Frink, J. Chem. Phys. **118**, 7457 (2003).
[28] D. G. Anderson, "Iterative procedures for nonlinear integral equations," J. Assoc. Comput. Mach. **12**, 547 (1965).
[29] Y.-X. Yu and J. Wu, J. Chem. Phys. **117**, 10156 (2002).
[30] R. Roth, R. Evans, A. Lang, and G. Kahl, J. Phys.: Condens. Matter **14**, 12063 (2002).
[31] Y. Rosenfeld, Phys. Rev. Lett. **63**, 980 (1989).
[32] A. R. Denton and N. W. Ashcroft, Phys. Rev. A **39**, 426 (1989).
[33] S. C. Kim and S. H. Lee, J. Phys.: Condens. Matter **16**, 6365 (2004).
[34] Z. Tang, L. E. Scriven, and H. T. Davis, J. Chem. Phys. **95**, 2659 (1991).
[35] S. S. Sokołowski and J. Fischer, J. Chem. Phys. **96**, 5441 (1992).
[36] J. Winkelmann, J. Phys.: Condens. Matter **13**, 4739 (2001).
[37] D. Frenkel and B. Smit, *Understanding Molecular Simulation from Algorithms to Applications* (Academic, San Diego, 1996).
[38] A. Malijevský, J. Chem. Phys. **126**, 134710 (2007).
[39] M. Knepley, A. Karpeev, S. Davidovits, R. Eisenberg, and D. Gillespie, J. Chem. Phys. **132**, 124101 (2010).